ECO-UW IoT: Eco-friendly Reliable and Persistent Data Transmission in Underwater Internet of Things

Mehdi Rahmati, Vidyasagar Sadhu, Dario Pompili
Department of Electrical and Computer Engineering, Rutgers University–New Brunswick, NJ, USA
{mehdi.rahmati, vidyasagar.sadhu, pompili}@rutgers.edu

***Abstract*—Achieving reliable and persistent environmental field estimation in Underwater Internet of Things (UW IoT) is a challenging problem. Given the need for high-resolution spatio-temporal sensing in such environment, traditional digital sensors are not suitable due to their high cost, high power consumption, and non-biodegradable nature. Further, reliable communication techniques that avoid retransmissions are crucial for reconstructing the phenomenon in a timely manner at the fusion center such as a drone. To address the above challenges, we propose a novel architecture consisting of a substrate of densely deployed underwater all-analog biodegradable sensors that continuously transmit data to the surface digital buoys. The analog nodes are designed to be energy efficient by implementing Analog Joint Source Channel Coding (AJSCC), a low-complexity compression-communication technique, using biodegradable Field Effect Transistors (FETs). We then propose a correlation-aware Hybrid Automatic Repeat Request (HARQ) technique to transmit data from the surface buoys to the fusion center. Such HARQ technique leverages redundancy in the buoy data (arising from the correlation of the phenomenon at the analog nodes) to avoid retransmissions, thus saving energy and time. The performance of the proposed analog sensor design and of the correlation-aware HARQ communication technique has been evaluated via simulations and shown to achieve the desired behavior.**

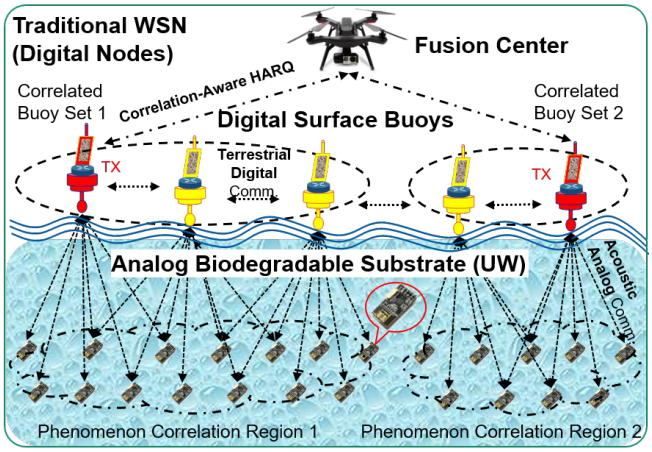

Fig. 1: A novel sensing architecture for real-time, persistent water monitoring using biodegradable analog sensors with Analog Joint Source-Channel Coding (AJSCC) capabilities as substrate above which lies the traditional Wireless Sensor Network (WSN) consisting of digital surface buoys drifting on the water communicating among themselves and occasionally to a fusion center (e.g., drone) using correlation-aware Hybrid Automatic Repeat Request (HARQ) technique to reduce costly retransmissions.

I. Introduction

Overview: The Underwater Internet of Things (UW IoT) [1] is a novel class of IoTs enabling various practical applications in aqueous environments such as oceanographic data collection, pollution and environmental monitoring, tsunami detection/disaster prevention, assisted navigation, and tactical surveillance [2], [3]. A new design has to be envisioned for sensors/things in UW IoT as traditional digital sensors are expensive (cannot be deployed in high density), high-power consuming (need to be put to sleep, thus losing temporal granularity), and finally pollute the environment. Moreover, similarity/correlation can generally be observed both in the underwater phenomenon as well as in the channel used for communication, which can be leveraged to improve efficiency.

Motivation: Firstly, for the UW IoTs to be a successful technology, the "things" or sensors should be able to capture high temporal and spatial variations of multiple manifestations—such as temperature, salinity, potential Hydrogen (pH)—of the phenomenon in the underwater environment. This requires high-resolution (in both time and space) sensing. Traditional digital sensors may not be the right candidates for such scenarios, as they: (i) Have high power consumption, because of which they are put to sleep based on specific duty cycles; moreover, existing sensor-encoding solutions use all-digital hardware, which demands high power and circuit complexity; as such, when the phenomenon exhibits high temporal variation, their batteries drain fast. (ii) Are expensive, making them a costly choice for high-density deployment, which is needed to track a phenomenon with high spatial variation. (iii) May pollute when deployed in water bodies as the material used in the manufacturing of such sensors is not biodegradable; currently, most electronics are typically made with nondecomposable, nonbiocompatible, and sometimes even toxic materials, leading to ecological challenges.

Secondly, when the sensors are densely deployed, the recorded values may be spatially and/or temporally correlated. Since communication of a large amount of measured data between the nodes results in large overhead (in terms of energy, time, and bandwidth), conventional point-to-point communication techniques at the physical and Multiple Access Control (MAC) layers generally fail to provide the required functionalities for such scenarios [4]. A reliable communication technique that takes into account the spatial and temporal correlations of the phenomenon to avoid costly retransmissions and thereby save energy and time resources is greatly needed.

Our Vision: To address the above challenges, we envision an architecture for the UW IoT system, as shown in Fig. 1, where the analog nodes in the underwater biodegradable substrate transmit data continuously to the digital surface buoys in the traditional Wireless Sensor Network (WSN), which aggregate and transmit the data to the fusion center (e.g., a drone). The underwater analog biodegradable substrate consists of wirelessly-transmitting all-analog sensors with Shannon-mapping [5] capabilities, a low-complexity technique for Analog Joint Source-Channel Coding (AJSCC) [6]. We

978-1-7281-1207-7/19/$31.00 ©2019 IEEE

propose an ultra-low power realization of Shannon mapping using characteristics unique to semi-conducting devices (specifically the input-output relation of a single Metal Oxide Semiconductor Field Effect Transistor (MOSFET) transistor), so that the sensors can be powered using only sustainable energy-harvesting techniques rather than polluting metal batteries. Such low-power/low-cost design allows sensors to be deployed in high density (thus enabling high spatial resolution) and also to sense continuously without the need to go into sleep modes (thus enabling sensing persistence/high temporal resolution). Since our analog nodes rely on energy-harvesting techniques to power themselves, they cannot afford long-range transmissions, i.e., that they need to be close to the buoys.

The sensors employ Frequency Position Modulation and Multiplexing (FPMM) [7], which allocates a specific frequency to a specific value of a specific node to communicate with the surface buoys. Biodegradable Micro Electro-Mechanical Systems (MEMS)-based acoustic transceivers with ranges of few meters are a perfect fit to our scenario. The digital surface buoys decode the values received from the analog sensors, i.e., they perform the reverse operation of Shannon mapping. Since the data received at the surface buoys could be redundant (due to correlation in the underlying phenomenon), as shown in Fig. 1, the digital buoys elect some of them to be "representatives" of the other buoys. Only these representative buoys transmit data to the drone (indicated in red as TX in Fig. 1). Further, the representative buoys employ a novel correlation-based closed-loop Hybrid Automatic Repeat Request (HARQ) solution to transmit data to the drone. Such a technique leverages the similarity and correlation of the data to avoid costly retransmissions and thereby save energy, time, and bandwidth resources, thus enabling a timely reconstruction of the phenomenon at the fusion center.

Our Contributions: Our contributions are as follows.

- We propose to use a MOSFET's drain-source current (I_{DS}) vs. drain-source voltage (V_{DS}) and gate-source voltage (V_{GS}) characteristic curves as a space-filling curve to perform Shannon 2:1 mapping, where I_{DS} encodes V_{DS} and V_{GS} values, resulting in a low-power/low-complexity all-analog encoding/compression technique.
- We introduce a reliable correlation-based HARQ to transmit data between the buoys and the drone that leverages the correlation of the data to avoid costly retransmissions; we adopt chaotic Direct Sequence Spread Spectrum (DS-SS) to guarantee secure buoy-drone transmissions.
- We validate the proposed sensor-encoding and correlation-aware HARQ techniques in terms of functionality using Spice and MATLAB simulations.

Paper Outline: In Sect. II, we go over the state of the art and similar research in the literature. In Sect. III, we discuss our proposed solution including the low-power, low-cost sensor design needed for the analog biodegradable substrate and the proposed correlation-based HARQ technique. In Sect. IV, we present the simulation results and discuss the benefits of our solution. Finally, in Sect. V, we draw the main conclusions and discuss our future work.

II. Related Work

We position here our work with respect to state-of-the-art research in low-power, low-cost sensor design, and reliable UW and terrestrial communication/channel coding techniques.

Sensor Design: All of the existing realizations of AJSCC [7], [8] are in the digital domain [9], except [10] where Zhao et al. proposed an analog circuit realization of AJSCC using Voltage Controlled Voltage Sources (VCVS) and Analog Dividers resulting in power consumption of the order of $90\ \mu$W. This is still high (considering additional overheads) to be powered with energy-harvesting techniques, which produce few 10's of μW [11]. On the energy-harvesting front, Toma et al. [12] proposed an underwater energy-harvesting system based on plucked-driven piezoelectric system with a maximum power density of $0.35\ \mu W/mm^3$. There is ongoing research work in the domain of biodegradable electronics. For example, Bao's research group [13] developed water stable Organic Field Effect Transistors (OFETs) for aqueous sensing applications. There are also works in the domain of ultra-low power transceivers [14] and, in particular, biodegradable MEMS transceivers for our sensors. Kim et al. [15] presented ultra-low power transistor-based transceiver designs with power consumption of the order of $50\ \mu$W and a range of a few meters. For more related work in the above domains, refer to [8]. All these works suggest that our vision of analog biodegradable sensors that are ultra lightweight, low power, and low cost as the sensing substrate is a feasible approach.

Reliable Communications: To improve the accuracy and efficiency of a system that exhibits spatial and temporal correlations [16], an Error Control (EC) strategy with acknowledgment such as Hybrid Automatic Repeat Request (HARQ) [17], [18] can be exploited. A type-I HARQ discards the erroneous received packet and repeats the same packet retransmission until the error is corrected. However, if the channel is not in good condition, e.g., when in deep fade, the predefined FEC might not be adequate and the throughput may drop again because of multiple retransmissions [19]. While more efficient than type-I, a type-II HARQ requires a larger buffer size and has a higher complexity. It adapts itself with the channel in such a way that it first transmits the packet along with the error detection bits when the channel is good. When the channel becomes worse and after detecting the erroneous packet, a NACK is sent back and—rather than retransmitting the same packet as type-I does—FEC information is transmitted to help decode the stored packet in the receiver's buffer. If the error persists, a second NACK is issued and the same FEC might be retransmitted or extra FEC might be added depending on the coding strategy. Incremental Redundancy (IR) HARQ, which shows a higher throughput efficiency in terrestrial time-varying channels, adds extra redundant information in each round of retransmission after receiving the NACK message [20]. Terrestrial standards such as High Speed Packet Access (HSPA) and Long Term Evolution (LTE) have exploited HARQ synchronously for the uplink, and asynchronously in the downlink direction. The requirements for designing a network-optimized HARQ for the fifth generation (5G) of mobile communications is discussed in [21]. Given the necessity of supporting futuristic applications such as UW IoT, we believe that a new design for HARQ that leverages the correlation in the data is essential.

III. Proposed Solution

In this section, we explain the important constituents of our architecture viz., energy-efficient analog biodegradable substrate (Sect. III-A) and the correlation-based HARQ tech-

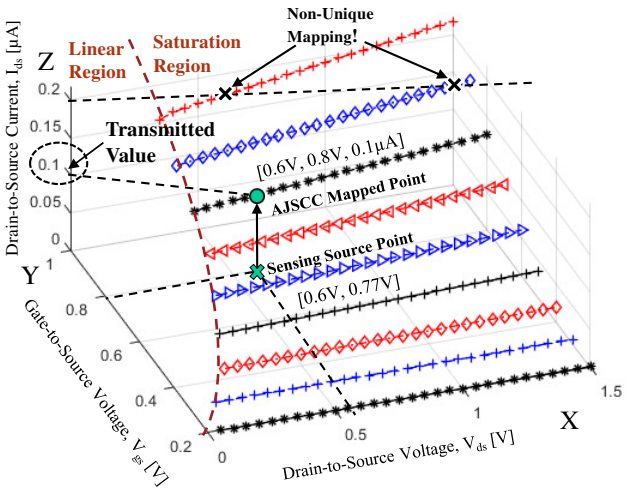

Fig. 2: 2D Shannon mapping (2:1 compression) realized via output characteristics (I_{ds} vs. V_{ds} for different V_{gs}) of a MOSFET in saturation region.

nique that leverages the correlation in the buoy data to avoid retransmissions between the buoys and the drone (Sect. III-B).

A. Energy-efficient Analog Biodegradable Substrate

We introduce here AJSCC and preset our novel idea of using MOSFET to realize rectangular AJSCC; we then describe the communication technique adopted by analog sensors to transmit data to buoy, followed by decoding and localization of the analog nodes at the buoy.

Analog Joint Source Channel Coding (AJSCC): Joint Source-Channel Coding (JSCC), also known as Shannon mapping [5], compresses two (or more) signals into one. JSCC achieves this using a space-filling curve where the x-axis signal is continuously captured while the y-axis one is quantized (let us denote the amount of quantization as ϕ). The sensed (x, y) point is mapped to the closest point on the curve and the encoded (compressed) value is a property of the curve, e.g., length of the curve from the origin to the mapped point. To achieve the low-power/low-complexity advantages of JSCC, this technique needs to be realized in the analog domain—hence the name Analog JSCC or AJSCC [9]. However, AJSCC is hard to realize on hardware in a power-efficient manner; this is especially important when the sensors are powered using energy-harvesting techniques [11].

FET-based Encoding at Transmitter: Power is of utmost importance in biodegradable sensors as they are powered using energy-harvesting techniques that can deliver power of the order of ten's of μW. Hence, there is a need to realize a simple implementation of AJSCC for substrate sensors. To this end, we present the idea of using a FET device's output characteristics to perform the encoding. Ideally, any new space-filling curves for AJSCC should preserve these properties: (i) they should achieve better trade-off between channel noise/compression and approximation noise; (ii) they should be realizable using *all-analog* components; and (iii) they should result in a *unique* mapping (i.e., two or more sensor values should map to *only one* AJSCC encoded value). Given these desirable properties of a space-filling curve, we propose the idea of using the IV (current-voltage) characteristics of a MOSFET as the space-filling curve (instead of using rectangular parallel lines as in [10]). A MOSFET has three terminals: Gate (G), Drain (D), and Source (S). When a suitable voltage is applied across the G and S terminals, V_{gs}, and the D and S terminals, V_{ds}, a current is generated across the D and S terminals, I_{ds}. The relationship between V_{gs}, V_{ds}, and I_{ds} for a *real* MOSFET in the saturation region (Fig. 2) is,

$$I_{ds} = \frac{1}{2} \cdot \frac{W}{L} \cdot \mu C_{ox} \cdot (V_{gs} - V_{th})^2 \cdot (1 + \lambda V_{ds}), \qquad (1)$$

where W, L [m] are width and length of the MOSFET channel, respectively, μ [m^2/Vs] is the electron mobility in the channel, C_{ox} [F/m^2] is the oxide capacitance per unit area, and λ [V^{-1}] is the Channel Length Modulation (CLM) parameter. Because of CLM, I_{ds} keeps increasing at a very slow rate (governed by V_{gs} and other parameters) as V_{ds} is increased in the saturation region. Fig. 2 shows these I_{ds} curves in the *saturation region* to the right of the dashed line (linear region curves are not drawn for clarity), generated via Spice, where V_{gs} is varied in the discrete set, $0.2, 0.3, ..., 1$ V (28 nm Silicon technology MOSFET is used for illustration purpose). We notice that the slope of the current curves increases as V_{gs} increases due to CLM, which we leverage to perform the decoding at the receiver, as explained below. I_{ds} encodes the values of V_{gs} and V_{ds} (as opposed to extracting the length of the curve from the origin to the mapped point, as in [10]). It is necessary to have a discrete set of y-axis (V_{gs}) values, and the actual y-axis value is mapped to the nearest value from the set and applied to the MOSFET to generate the encoded current (Fig. 2).

We propose the idea of using these saturation-region characteristics of a MOSFET with channel length modulation to fill the space, where I_{ds} encodes the values of V_{gs} and V_{ds} It should be noted that the *shape* of the output characteristics (I_{ds} vs. V_{ds} for different V_{gs}) of a biodegradable MOSFET is similar to that of regular Silicon MOSFET (as shown in [22]). Moreover, the current generated of the polymer MOSFET in [22] is of the order of few μA; with a supply voltage of 1 V, this will result in few μW of power consumption, which can be supported by energy-harvesting techniques. While the proposed MOSFET-based space-filling technique satisfies (i) and (ii) properties mentioned above, it violates (iii) as a given I_{ds} value could be generated from multiple pairs of V_{gs} and V_{ds} values as illustrated in Fig. 2. This is problematic as it is difficult to decode the correct V_{gs} at the receiver. To address this challenge, we propose a decoding technique at the digital receiver based on the previously received I_{ds} value.

Frequency Position Modulation and Multiplexing: The analog sensors will be communicating to the receiver (digital buoy) using Frequency Position Modulation and Multiplexing (FPMM) as explained below. Assume that there are N analog nodes communicating with a digital buoy (i.e., the buoy is within the communication range of the analog nodes). Assume the AJSCC encoded I_{ds} current values at each analog node are quantized into Q levels and the total available bandwidth is B. This bandwidth is then divided into $N \times Q$ frequency bins, and each bin is assigned to a particular value of a particular node. Assume V_{nq} represents the value level, q, of node n, where $q \in \{1, ..., Q\}$ and $n \in \{1, ..., N\}$. The assignment of frequencies to values and nodes is such that same value level of all nodes, i.e., frequencies corresponding to $\{V_{1q}, ...V_{Nq}\}$ for any q, are adjacent to each other (call it a frequency band) to ensure lower interference. While a linear mapping can be done between value levels and frequency

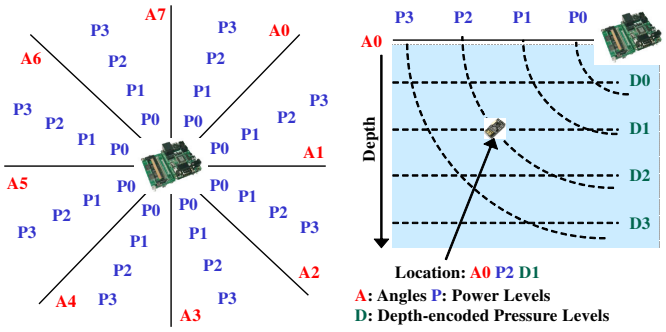

Fig. 3: Localization of sensors into *subregions* by the buoy based on directionality ("A"), received power ("P"), and depth-encoded pressure ("D").

bands, such simplistic mapping can pose two problems: (i) if the phenomenon is correlated and all the nodes sense same value, their frequencies are close to each other; if an interference happens at the location of these frequencies, all data is lost; (ii) susceptible to eavesdropping. Consequently, it is desirable to design an analog scrambling mechanism [23] that scrambles the assignment of frequencies to values in a random manner that is known only between the nodes and the receiver.

Decoding at Receiver: We assume that the discrete set of V_{gs} values used at the analog nodes for encoding is known at the digital receiver. The decoding process relies on the assumption that physical values do not change abruptly and hence two consecutive received I_{ds} values at the receiver will lie on the same I_{ds} curve (i.e., corresponding to a particular V_{gs} value). The probability of them lying on different I_{ds} curves (i.e., corresponding to different V_{gs} values) is low as the two consecutive values would have sensed similar values (i.e., the sampling rate at the sensor is more than the rate of change of the phenomenon), would have experienced similar wireless channel conditions (i.e., the sampling rate at the sensor is more than the rate of change of channel) and hence would belong to the same I_{ds} curve. The challenge then lies in identifying the correct V_{gs} value out of the discrete set of V_{gs} values used at the transmitter using these two consecutive I_{ds} values. For this purpose, we designed a *slope-matching technique* as follows. We calculate slope 1 using (1) and slope 2 assuming all possible values for V_{gs} and using the geometric two-point formula. Slope 1 can be calculated as $\lambda \cdot (I_{ds}^{(1)} + I_{ds}^{(2)})/2$. For all the possible V_{gs} values, the receiver solves for $V_{ds}^{(1)}$ and $V_{ds}^{(2)}$ from $I_{ds}^{(1)}$ and $I_{ds}^{(2)}$. Then it calculate slope 2 using the two-point formula. We then choose that V_{gs} whose slope 2 matches closest with slope 1 and with its corresponding V_{ds} (for $I_{ds}^{(2)}$) as the decoded V_{gs} and V_{ds} values.

Quantization and Power Consumption: For the above decoding to work, it is necessary that the V_{gs} is quantized at the transmitter before feeding to MOSFET. We have designed a precircuit in [24], that quantizes V_{gs} at multiple quantization levels. Specifically, for 9 levels, the power consumed is ≈ 24 μW, with possibility of 8 μW. Transmission power is around 50 μW using MEMS-based transceivers with a range of few meters [24]. Hence our sensors can be powered using energy-harvesting techniques, which produce tens of μW [24].

Localization at Receiver: Localization of sensor nodes at the buoy is essential to help visualize how the phenomenon varies with space and time. However, the traditional approach of assigning unique IDs to nodes entails additional cost and overhead and is also unscalable [25]. We instead propose a scalable location inference technique that uses a combination of three methods—directionality, received power, and depth-encoded pressure, as shown in Fig. 3. We will now illustrate these three techniques using a simple example. Since the buoy is digital, we assume it can determine the direction of the received signal using specialized hardware such as acoustic vector sensors. For illustration, assume it is able to distinguish among eight directions/angles, indicated as $A_0, ..., A_7$, in Fig. 3. Next, if the nodes transmit with a fixed amount of power, the power level of the signal received by the buoy at short ranges varies with the distance between the buoy and the node [26]. Assume the buoy is able to distinguish among four received power levels, $P_0, ..., P_3$. Finally, it is well-known that the pressure varies with depth. The buoy can extract this information if the nodes sense pressure for V_{gs} (along with other manifestations such as Salinity for V_{ds}). This can be done only occasionally using a simple analog timing circuit. Since the final AJSCC encoded (I_{ds}) values are quantized to Q levels as mentioned above, the buoy can only distinguish among, at maximum, Q pressure levels. These are indicated as $D_0, ..., D_3$ in Fig. 3 for $Q = 4$. The pressure levels help reduce the location uncertainty for a given angle and power level, as shown in Fig. 3. Within a given angle level (A_0) and power level (P_2), it is possible that the sensor could lie anywhere on the dashed curve originating at P_2. However, since the pressure/depth level corresponds to D_1, the uncertainty has been reduced. We call the largest area that can be localized using a combination of these three methods as a *subregion*. The buoy, upon localizing all its analog nodes into the above subregions, averages the (decoded) values of all nodes within the same subregion. Instead of transmitting the data from all the subregions to the drone, the buoys first estimate the correlations among the subregion data and elect among themselves certain representatives (called transmitter buoys), i.e., only those whose data is transmitted to the drone. A correlation-aware HARQ technique is used between the buoys and the drone to avoid costly retransmissions which is explained in the following section.

B. Correlation-based HARQ Technique

In this section, we present our correlation-based HARQ, which employs a chaotic DS-SS to avoid interference.

Spatial and Temporal Correlations: Let $n_i, \{i = 1, ..., N\}$ denote N subregions with the location index $L_i \in \mathbb{L} \subset \mathbb{R}^3$, where $\mathbb{L}$ denotes the 3D environment's space. The data is shown by matrix $\mathcal{P} = [P_1, ..., P_N]$. The ith column of $\mathcal{P}$, corresponding to subregion L_i, consists of data from the K manifestations, i.e., $[\mathcal{P}]_i = P_i = [\psi_i^{(1)}(t), ..., \psi_i^{(k)}(t), ..., \psi_i^{(K)}(t)]$.

Definition 1. *For the subset of* ***interconnected*** *subregions $\mathcal{L}_i$, $\{i = 1, ..., \mathcal{N}\} \subset \mathbb{L}$, let the spatial correlation between two sampled values $\psi_i^{(k)}(t)$ and $\psi_j^{(k)}(t)$ with means $\underline{\psi}_i^{(k)}$ and $\underline{\psi}_j^{(k)}$ and standard deviations $\sigma_i^{(k)}$ and $\sigma_j^{(k)}$, at time t, be as*

$$C_{i,j}^{(k)} = \frac{\mathbb{E}\big[(\psi_i^{(k)} - \underline{\psi}_i^{(k)})(\psi_j^{(k)} - \underline{\psi}_j^{(k)})\big]}{\sigma_i^{(k)} \sigma_j^{(k)}}, \qquad (2)$$

where $\mathbb{E}[.]$ represents the expectation value and the time notation is dropped for simplicity.

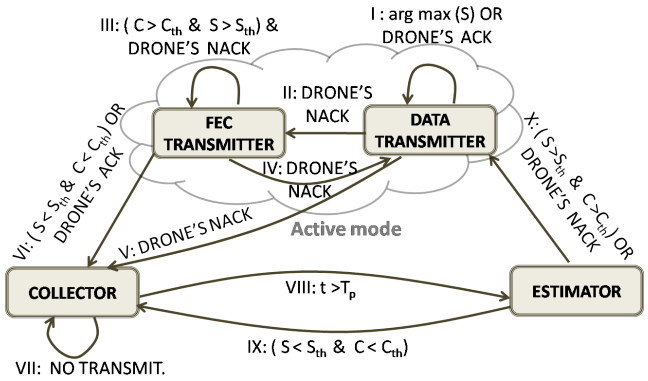

Fig. 4: State transition diagram for a buoy in a correlated set. In the active mode, i.e., $(I)-(IV)$, the buoy starts the HARQ process with the highest similarity chosen as the data transmitter. If a NACK is issued, whether the FEC transmitter is chosen via (II), or the buoy becomes a collector via (V). If FEC fails, the data is dropped and the next data is transmitted via (IV). If the correlation and similarity of data transmitter drop below a threshold, it demotes to a collector via (VI), until the estimator is activated after a specific time via $(VIII)$ to check whether it is qualified to switch the role.

Definition 2. *Let the spatial correlation be a function $\mathcal{F}(.)$ of the distance between two locations $\mathcal{L}_i$ and $\mathcal{L}_j$ as in $\mathbb{E}\big[(\psi_i^{(k)}-\underline{\psi}_i^{(k)})(\psi_j^{(k)}-\underline{\psi}_j^{(k)})\big]=\mathcal{F}(\mathcal{L}_i-\mathcal{L}_j)$. The subregions are correlated when $C_{i,j}^{(k)} > C_{th}^{(k)}$, where $C_{th}^{(k)}$ is the spatial correlation threshold. The correlation matrix for the manifestation k is symmetric and is defined by $[\mathbb{C}^{(k)}]_{i,j}=C_{i,j}^{(k)}$.*

Definition 3. *The measured data of a manifestation k in subregions i and j are said to be similar if the normalized difference of their means is less than a threshold $(1-S_{th}^{(k)})$, where $S_{th}^{(k)}$ is the similarity threshold, i.e., $1-|\,\underline{\psi}_i^{(k)}-\underline{\psi}_j^{(k)}\,|/\underline{\psi}_j^{(k)} > S_{th}^{(k)}$.*

Definition 4. *Temporal correlation is defined as the degree of correlation for which two consecutive sampled data at the buoy are correlated. In other words, the amount of correlation does not change within the time $\tau < T_{\mathcal{P}}^k$, where $T_{\mathcal{P}}^k$ is the temporal correlation of the k-th manifestation. It can be concluded that $C_{i,j}^{(k)}(t+\tau)=C_{i,j}^{(k)}(t)$ and so the expectation of the random variable ψ_i is constant.*

Each buoy at a time has one of the roles of a *data transmitter/FEC transmitter* (active mode), a *collector*, or an *estimator*. The transition among the roles is decided by the phenomenon's correlation/similarity and also the feedback command given by the drone as shown in the state diagram, Fig. 4. Data transmitter role is decided based on two factors: the highest similarity, $\arg\max(\mathrm{S_{i,j}})$, and spatial correlation greater than a threshold $C_{i,j} > C_{th}$; the control command from the drone. If the data transmission is not successful and the drone issues a NACK, the buoy's state will change from data transmitter to FEC transmitter as shown in (II). Drone could turn the buoy's role to a collector if it decides to not receive any data from the same buoy, as shown in (V) and (VI). An estimator is a collector that has started to evaluate whether its newly received data from analog nodes is still correlated and similar to that of its data transmitter buoy or not. It changes its state to become a data transmitter if there is a significant variation in the spatial distribution of its data over time as shown in (X). The two main communications aspects, *intra-cluster* communications (among the buoys) and *inter-cluster* (between the data/FEC transmitters and the drone) are discussed in the following sections.

Intra-cluster Chaotic-based Spread Spectrum: Code Division Multiple Access (CDMA), as both physical-layer and multiple-access techniques, can be beneficial to handle the destructive effect of frequency-selective fading, as well as the simultaneous reception from multiple transmitting devices by using an appropriate spreading, especially in an IoT network. Furthermore, given the security dedicated in chaotic CDMA's nature, the jamming attacks as a critical malicious threat can be satisfied [3]. Although Pseudo-Noise (PN) sequences have been extensively employed in DS-SS, considering their limitation in the number of sequences and their cross-correlation properties, [27] proposed using chaotic sequences through an uncomplicated deterministic dynamic map such as in Logsitic map [28]. Chaotic systems can produce an infinite set of uncorrelated sequences and can provide secure communication. Similar to the PN sequences, they look like noise but unlike PN, chaotic codes are not binary and are different for every bit of transmitted data which makes it much harder for an eavesdropper to regenerate the sequence. The use of a distributed CDMA scheme, supporting an adaptive EC strategy, can therefore increase the channel reuse and reduce packet retransmissions in scenarios with a large number of buoys, thus increasing network reliability while decreasing the energy consumption. While conventional EC strategies consider only point-to-point data protection, more efficient techniques are required in such applications in which (i) the buoys have some sort of similarities and correlations in time or space in the measured data; (ii) the importance of phenomenon monitoring is higher than protecting of each buoy alone; (iii) the communications overhead is huge—since multiple buoys communicate with each other and with the drone—and so a scheduling is required. To support reconfigurable and flexible IoT applications in which the number of simultaneous transmissions is not known in advance, chaotic sequences can be a good candidate to support any number of transmitters. Chaotic sequences not only provide the security in the channel, but also possess a considerable robustness due to their good auto-and cross-correlation properties.

Inter-cluster Correlation-based HARQ: The transmission process is conducted in an environment in which the phenomenon's manifestations change from time to time as represented by temporal and spatial correlations of the phenomenon. Therefore, an appropriate multi-point EC strategy should (i) take advantage of the defined correlations of data/FEC transmitter buoys versus collector and estimator buoys for efficient decoding by increasing the probability of successful decoding in each round; (ii) reduce the probability of retransmission and also the communications overhead with a correlation-based coding, while the temporal correlation of the phenomenon is long enough; (iii) pause the decoding process and go for the retransmission, while the temporal correlation of the phenomenon can not be ignored.

As portrayed in Fig. 5, buoys are shown on the left with numbers $1, 2, ...$ while the drone stands on the right side of the diagram. Each data transmitter buoy broadcasts its packets through independent channels to the other buoys and to the drone (within a single-hop distance). As an example, a conservative approach is taken in case (a), since no a-

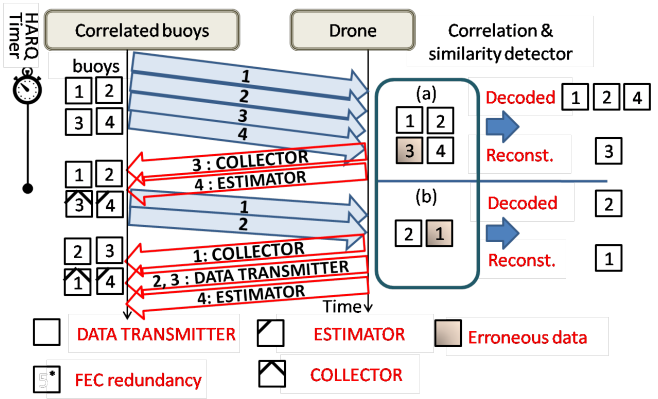

Fig. 5: Proposed protocol for data transmission to the drone via a correlated set of buoys—shown with numbers $1, 2, ...$ Spatial and temporal correlations are considered in decoding. Conservative and borderline approaches are compared in cases (a) and (b).

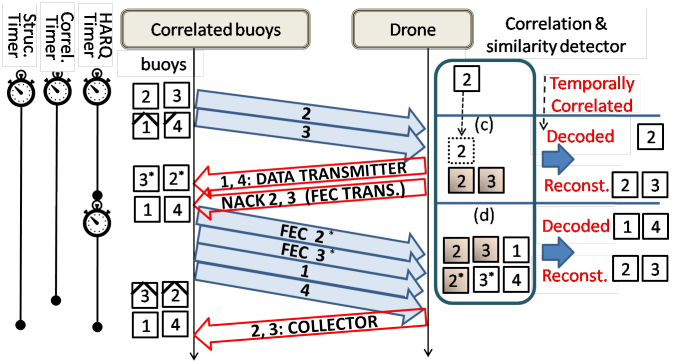

Fig. 6: Proposed solution when the packets are corrupted. Case (c) leverages the temporal correlation while case (d) uses spatial correlation via combined data and FEC. Three timers are defined; HARQ timer for each round of transmission; Correl. timer for the duration of temporal correlation; and structure timer for the time that the structure of the network is unchanged.

priori information is available beforehand. Assume the decoder successfully decodes all the packets, except 3. Here—instead of issuing a NACK as in the conventional HARQ—buoy 3's data can be reconstructed using the correlation among the other decoded data. The cost is the extra error in estimating the corrupted data; however, it can be ignored if buoys are highly correlated. In case (b), the borderline approach is considered to avoid the excessive redundancy (communications overhead) of case (a) and to reduce the interference by using only 1 and 2 as the data transmitter while 3 and 4 are changed to collector and estimator, respectively. Assume the data from 1 is erroneous while 2 is still decodable. Again, 1 is reconstructed without any extra FEC with the cost of more reconstruction error.

Fig. 6 presents two cases (c) and (d) in which both the received data—such as those of 2 and 3—are erroneous. The corrupted data is recoverable, if the temporal correlation of the phenomenon is valid at that time instant and available at the drone, as shown in case (c). If this condition does not hold—which is the scenario in case (d)—since the overall information is not enough for making the decision, 3 is notified to send the FEC information by switching to the FEC transmitter role. The extra information in 2^* and 3^*, combined with the data from 1 and 4, help the decoder to have both the conventional HARQ and the spatial correlation properties. Therefore, the decision is made on 2 and 3 based on the tolerable amount of reconstruction error in 3. We define three different notions of time in our coding scheme, as shown in Fig. 6. *HARQ timer*, T_{HARQ}, is used to show the transmissions/FEC transmission time (for erroneous packets) for every round of communications. *Correl. timer*, T_{Corr}, represents the time within which data transmission/decoding can be done consecutively based on the temporal correlation of the phenomenon. This time is less than or equal to $T_{\mathcal{P}}$. If the data is not acknowledged in T_{HARQ}, but $T_{Corr} >> T_{HARQ}$, then the data can be recovered without retransmission as explained in case (c). *Struc. timer*, T_{Stru}, is the time in which the structure is almost constant. Therefore, outside of this time period, the correlated sets should be reconsidered, because of the analog node movement. In this case, the extra FEC or using the correlation might not be helpful; therefore, the retransmission of the original/new data using new set of buoys will be the solution for time $t > T_{Stru}$.

Data Reconstruction: Based on the renewal-reward theorem [29], let the HARQ long-term throughput for buoy i be $\eta_i = \mathbb{E}[\tilde{X}_i]/\mathbb{E}[\tilde{T}_i]$, where $\mathbb{E}[\tilde{X}_i]$ and $\mathbb{E}[\tilde{T}_i]$ represent the number of decoded information nats and the number of attempts for channel use during a packet transmission period for buoy i, respectively. $\mathbb{E}[\tilde{X}_i]$ is defined as $\mathbb{E}[\tilde{X}_i] = X_i(1 - \overline{\Pr_{o(i)}})$, in which X_i is the number of information nats for a packet and $\overline{\Pr_{o(i)}}$ denotes the probability that the data is not decodeable during a packet transmission period. We consider an alternative packet which comes from a correlated buoy j with the correlation coefficient $C_{i,j}$, and $\overline{\Pr_{o(j)}} < \overline{\Pr_{o(i)}}$, i.e., the communication channel that j experiences is better than i's channel. We conclude that $R_j < R_i$, where R stands for the maximum number of transmission rounds in the HARQ. The probability of decoding in round R_i for buoy i given that the data has not been decoded in the previous $R_i - 1$ rounds is equivalent to $\Pr\left(\mathrm{NACK}_1, ..., \mathrm{NACK}_{\mathrm{R_i}-1}, \mathrm{ACK}_{\mathrm{Ri}}\right)$. Assume at every round r, for all the acknowledged buoys in the same correlated set, there exists at least a buoy j, where $R_j < R_i$. j is chosen as $\arg\max\ \mathrm{C_{i,j}}$. Therefore, $R'_i = \min[\mathrm{R_i}, \mathrm{R_j}]$ and so it is a function of the correlation between i and j. Then, $\mathbb{E}[\tilde{T}_i]$ can be defined as $\mathbb{E}[\tilde{T}_i] = \sum_{r=1}^{R'_i} X_{i\,r} \Pr\left(\mathrm{NACK}_1, ..., \mathrm{NACK}_{\mathrm{r}-1}, \mathrm{ACK}_{\mathrm{r}}\right)$, where $X_{i\,r}$ stands for the part of HARQ data which is transmitted at round r from buoy i. $\mathbb{E}[\tilde{T}_i]$ can be simplified in two terms as $\mathbb{E}[\tilde{T}_i] = \sum_{r=1}^{R'_i-1} X_{i\,r} \Pr\left(\mathrm{NACK}_1, ..., \mathrm{NACK}_{\mathrm{r}-1}\right) + \mathbf{X}_{\mathrm{j\,R'_i}} \Pr\left(\mathrm{NACK}_1, ..., \mathrm{ACK}_{\mathrm{R'_i}}\right)$ [30]. Here, the total data transmission from buoy j up to the end of round R'_i is shown with $\mathbf{X}_{j\,R'_i} = \sum_{r=1}^{R'_i} X_{j\,r}$. The content of $\mathbf{X}_j$ is correlated with X_i within the temporal correlation $T_{\mathcal{P}}$. Since their data are not exactly equal, this leads to an uncertainty related to the amount of $C_{i,j}$ with the benefit of avoiding $R_i - R'_i$ rounds of HARQ retransmissions and having a better long-term throughput.

When the data is transmitted from buoy i to the drone, it is polluted with the noise and affected by the fading and the interference. We assume the received signal $\hat{X}_i$ at the drone follows an Autoregressive time series model of order one, i.e., AR(1). That is at time instant t_m, $\hat{X}_i[t_m] = \mu + \rho(\hat{X}_i[t_m - 1] - \mu) + \epsilon_i$, where μ is the mean of $\hat{X}_i$, ϵ_i is a zero mean unit variance independent Gaussian process, and ρ is the autoregression parameter which is related to the temporal correlation of the phenomenon. Assume we take $\mu = 0$ for the sake of simplicity. For $-1 < \rho < 1$ and for any discrete

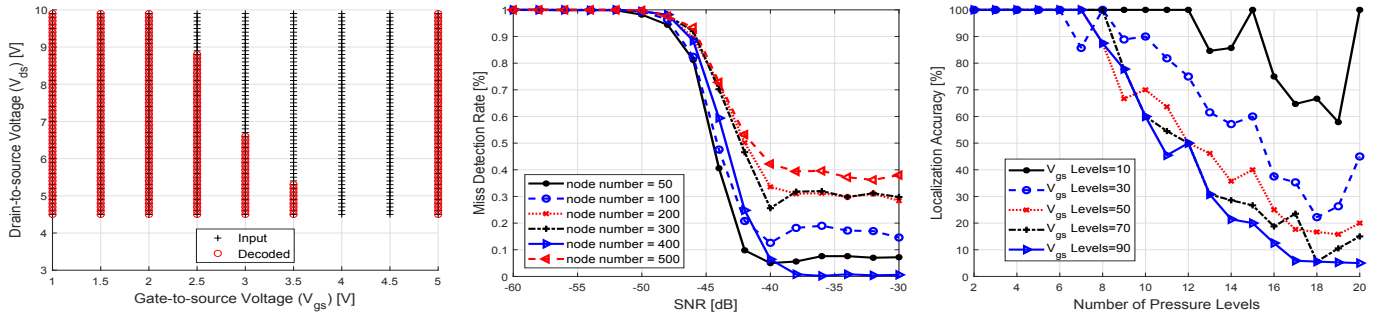

(a) (b) (c)

Fig. 7: (a) Decoding results for $\phi = 0.5$ V when no correction logic is used; (b) Miss Detection Rate vs. SNR as the number of nodes is varied; (c) Localization accuracy vs. number of pressure levels as the number of AJSCC quantization (V_{gs}) levels are varied.

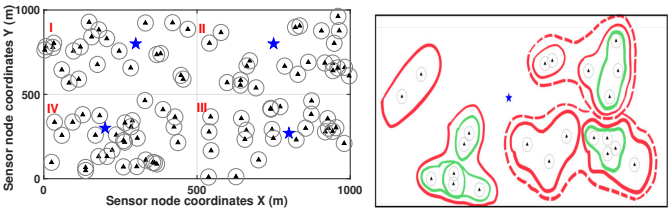

(a) (b)

Fig. 8: (a) Digital nodes (buoys) random distribution on the water surface (▲). Drone (★) passes by each region (shown by Roman numbers) to fuse the data; (b) Magnified view of region II with different degrees of correlation. Different colors show how the buoys are correlated.

time lag t_0, $\mathrm{Cov}(\hat{\mathrm{X}}_\mathrm{i}[\mathrm{t_m}+\mathrm{t_0}], \hat{\mathrm{X}}_\mathrm{i}[\mathrm{t_m}]) = \rho^{\mathrm{t_0}}/(1-\rho^2)$ [31]. Here $\hat{X}_i[t_m], \hat{X}_i[t_m-1], \ldots$ form a Markov process given that channel coherence time (T_c) is greater than the time window between two successive received samples t_m and t_{m-1}. Note that in addition to the noisy measured data by analog nodes, other layers of error are added to the data when it is received by the drone. Therefore, the difference between the measured value of the transmitter buoy and other buoys in the same correlated set is not zero. The transmitted data from ith transmitter buoy can be written as $\mathcal{P} + \mathcal{E}_{s,i} + \mathcal{E}_{c,i}$, where $\mathcal{E}_{s,i}$ and $\mathcal{E}_{c,i}$ represent the sensing error and communications error related to the transmitter buoy i, respectively. This signal is transmitted through channel h_i and is received at the drone as $\hat{X}_i$. The phenomenon can be estimated as $\widehat{\mathcal{P}} = F\big(\sum_{i=1}^{R} \hat{X}_i + \mathcal{N}\big)$, where $F(.)$ represents a data extraction function, and $\mathcal{N}$ is the background AWGN noise present in the environment. Therefore, the reconstruction error, $\mathcal{E}_{rec}$, is defined as $\mathcal{E}_{rec} = \left|\mathcal{P} - \widehat{\mathcal{P}}\right|$. Considering the number of buoys transmitting in each round of transmission, the goal is to increase the performance by reducing the communications overhead and destructive effect of other buoys, i.e., to minimize $\left\|\widehat{\mathcal{P}} - \mathcal{P}\right\|^2$, using appropriate channel coding.

IV. Performance Evaluation

We evaluate the performance of the proposed techniques via MATLAB and Spice simulations, first analog sensor design including FPMM and localization techniques (Sect. IV-A); and then the correlation-based HARQ technique (Sect. IV-B).

A. Analog Substrate and Buoy

MOSFET Encoding and Decoding: In order to evaluate the MOSFET-based encoding and decoding techniques, we used a 0.18 μm technology n-channel MOSFET (nMOS) with $W \cdot \mu \cdot C_{ox}/L = 155 \times 10^{-6}$ F/Vs, $V_{th} = 0.74$ V, $\lambda = 0.037$ V^{-1} in LTSpice simulation software. V_{ds} is varied from 4.5 to 10 V, in increments of 0.1 V. The reason not to start from 0 V is to ensure that the MOSFET is well into the saturation region. Discrete set of V_{gs} values in the range $[1, 5]$ V as per $\phi = 0.5$ V are considered, e.g., $V_{gs} = 1, 1.5, , ..., 5$ V; hence, for each V_{gs}, 55 values of V_{ds} are considered. Upon applying these voltages to the MOSFET, the generated I_{ds} values are recorded and sent to the digital receiver (no wireless channel), where the decoding process is done. At the receiver, each curve is processed independently and two consecutive I_{ds} values from the same curve are used for decoding the correct V_{gs} using the slope-matching technique. The results are shown in Fig. 7(a), where the original values are shown using '+' and decoded values using 'o'. We can see that some of the values are decoded incorrectly (where there are bare '+' without 'o'). The reason is due to mismatch between two slopes—the slope calculated theoretically, λI_{ds}, (varies with V_{ds}) is an approximation (i.e., valid only for $\lambda V_{ds} << 1$) of the actual slope calculated using the two-point formula (independent of V_{ds}). To solve this problem, we used a range-checking technique where, if the decoded V_{ds} value corresponding to the best (in terms of slope match) V_{gs} value does not fall within the V_{ds} range assumed at the transmitter $(4.5, 10)$ V, the next best V_{gs} value (in terms of slope match) is chosen and the process is repeated iteratively. Using this correction logic, we were able to improve decoding accuracy (100% for $\phi = 0.5$ V).

Frequency Position Modulation and Multiplexing: We studied the FPMM-based multiplexing for underwater channel conditions via MATLAB simulations. We have carried out simulations to find the miss detection rate of the system and how the noise affects it for different number of users (N_{user}), bandwidths and SNR values. We considered 50 V_{gs} levels and $Q = 100$ quantization levels of the final encoded I_{ds}. We used a Rician channel with single path (as the distance between the nodes and buoy is of the order of few meters), and a Doppler shift equal to 1% of the transmitting frequency (as the analog nodes could move underwater). Then, Additive White Gaussian Noise (AWGN) noise as per bandwidth (BW) and SNR considered is added. The received signal at the buoy has been recorded for 1 s, then passed through Fast Fourier Transform (FFT) analysis to find the peak frequency. We considered, Miss Detection Rate (MDR) as the metric

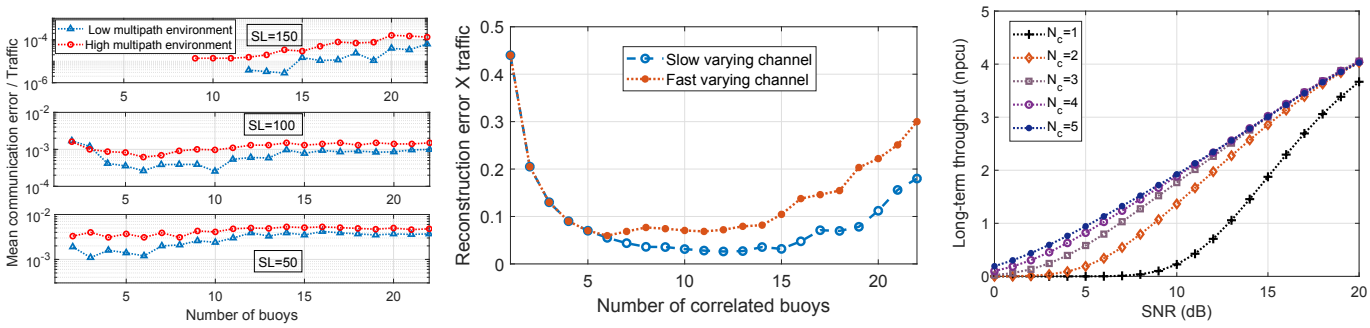

(a) (b) (c)

Fig. 9: (a) Mean communication error per traffic for buoys inside one region in low and high multipath while three different spreading length for the chaotic code are considered; (b) Reconstruction error $\times$ traffic for buoys inside a region while considering two different fading channel. (c) Long-term throughput of correlated HARQ, in nats-per-channel-use (npcu), for different number of data transmitter buoys.

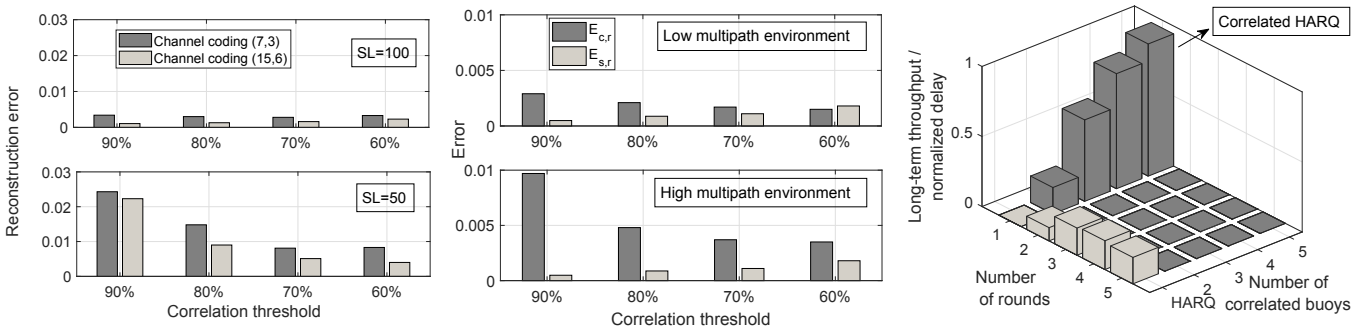

(a) (b) (c)

Fig. 10: (a) Reconstruction error for different correlation thresholds; comparing channel coding $(7, 3)$ and $(15, 6)$, in low multipath environment; (b) Sensing error and communication error for different correlation thresholds, in low and high multipath environments for chaotic code ($SL = 100$); (c) Long-term throughput per normalized delay for correlated HARQ versus number of rounds compared to the conventional HARQ.

of evaluation, defined as the number of users with detected frequency position not equaling the transmitting frequency position, divided by the total number of users multiplexed by FPMM. We have set the bandwidth to 10 KHz and varied the SNR from -60 dB to -30 dB and the number of nodes (N) from 50 to 500. The result is shown in Fig. 7(b), where, we can notice that the MDR falls to a low value for SNR=-40 dB. Due to the frequency modulation adopted, very low SNR can result in a detectable peak in frequency. We noticed that the MDR behavior is approximately same for other bandwidths considered (until 500 KHz).

Localization at Receiver: Since directionality and localization based on received power levels are well-studied in literature [26], we evaluated only the performance of the localization with respect to received (AJSCC encoded) pressure levels. We considered a distance of 5 m between points A and B, which is divided into equal number of bins equal to the number of pressure levels considered. An analog node is assumed to be present in the middle of each bin and encodes its distance from A into V_{gs}, while considering an arbitrary fixed $V_{ds} = 2.5$ V. These two values are then AJSCC encoded into I_{ds} by varying the number of V_{gs} quantization levels. The encoded I_{ds} is then transmitted to the buoy (without channel effect) which does AJSCC decoding using the slope-matching technique (a small variation in V_{ds} is assumed to generate two I_{ds} values needed by the slope-matching technique). If the decoded V_{gs} falls in the same bin as was used in the transmitter, it is considered a correct localization. Fig. 7(c) shows the percentage of correct localizations (i.e.,accuracy) as the number of pressure levels considered is increased for different number of V_{gs} quantization levels. We can notice that the accuracy drops as the number of pressure levels considered is increased. Interestingly, we can notice that, for about 10 pressure levels, a 100% accuracy can be achieved. Further, we can notice that accuracy increases (at the cost of higher quantization error) as the number of V_{gs} levels is reduced. This is because, the slope matching technique has less than number of levels to choose from, thereby reducing the probability of picking wrong V_{gs} level and hence increasing accuracy.

B. Buoy and Fusion Center

We consider an area of study with 100 randomly deployed buoys for the simulation, as represented in Fig. 8(a). We divide this area into four regions of interest; each of them shows a fusion center, the drone, passes by the region to communicate with the buoys and to fuse the collected data. The buoys are grouped based on their similarity and correlation. A magnified version of region II is displayed in Fig. 8(b). This figure also shows the various possible sets of correlated buoys based on different correlation thresholds. Data transmission is performed using Binary Phase Shift Keying (BPSK) modulation and Reed-Solomon coding $(7, 3)$ or $(15, 6)$ and CDMA spreading sequence with logistic map. As a general rule, spreading sequences should have minimal cross-correlation to minimize the interference between the buoys and a delta-function shape autocorrelation to maximize the detection accuracy of the desired buoy.

Fig. 9(a) investigates the performance of our method in terms of the mean communication error normalized by total traffic for different number of transmitter buoys. It compares the effect of changing the spreading length and presents the results when communication takes place in channels with different multipath effects. For $SL = 150$ when the number of buoys are small, the error is less than 10^{-6} (they are not depicted in the figure). The curves show communication error increases when the number of buoys grows (as the result of multi-user interference); however codes with larger SL are more successful in combating the multi-user interference. In Fig. 9(b) reconstruction error is presented for total traffic of the transmitter buoys. It also compares the effect of transmitting under slow and fast fading channels. Fig. 9(c) calculates the long-term throughput of the proposed HARQ for different number of correlated buoys. The correlation threshold is a determinant factor in evaluating the performance of the system. In Figs. 10(a)-(b), we investigate the effect of different correlation thresholds. In Fig. 10(a), reconstruction error is represented with HARQ channel coding $(7, 3)$ and $(15, 6)$. Fig. 10(b) presents two components of reconstruction error (sensing and communication errors). Fig. 10(c) shows the long-term throughput per normalized delay for correlated HARQ compared to the conventional HARQ.

V. Conclusion and Future Work

We proposed a novel architecture for UW IoT consisting of analog biodegradable substrate deployed underwater in high-density and transmitting data continuously to digital surface buoys. We then proposed a correlation-based Hybrid Automatic Repeat Request (HARQ) to transfer data between digital surface buoys and the fusion center that leverages the correlation in the data to avoid costly retransmissions and thereby enable timely reconstruction of the phenomenon. The proposed techniques have been evaluated via MATLAB simulations and shown to provide the desired performance. As future work, we plan to further reduce the power consumption of the analog nodes and test the initial prototype of the architecture in a lake setting. We consider the dynamic change in the structure and its effect on the proposed HARQ solution.

Acknowledgment: This work was supported by the US National Science Foundation (NSF) via the NeTS Award No. 1763964 and CPS Award No. 1739315.

References

[1] M. C. Domingo, "An overview of the internet of underwater things," *Journal of Network and Computer Applications*, vol. 35, no. 6, pp. 1879–1890, nov 2012.

[2] M. Rahmati and D. Pompili, "Ssfb: Signal-space-frequency beamforming for underwater acoustic video transmission," in *Proceedings of IEEE International Conference on Mobile Ad Hoc and Sensor Systems (MASS)*, 2017, pp. 180–188.

[3] M. Rahmati, D. Pompili, and R. Petroccia, "Collaborative hybrid ARQ for CDMA-based reliable underwater acoustic communications," in *Proceedings of IEEE Underwater Communications and Networking Conference (UComms)*, 2018, pp. 1–5.

[4] M. Rahmati and D. Pompili, "Probabilistic spatially-divided multiple access in underwater acoustic sparse networks," *IEEE Transactions on Mobile Computing, doi:10.1109/TMC.2018.2877683*, pp. 1–13, 2018.

[5] C. Shannon, "Communication in the presence of noise," *Proceedings of the IRE*, vol. 37, no. 1, pp. 10–21, 1949.

[6] F. Hekland, G. Oien, and T. Ramstad, "Using 2:1 Shannon mapping for joint source-channel coding," in *Proceedings of Data Compression Conference (DCC)*, 2005, pp. 223–232.

[7] X. Zhao, V. Sadhu, and D. Pompili, "Analog signal compression and multiplexing techniques for healthcare internet of things," in *Proceedings of IEEE International Conference on Mobile Ad Hoc and Sensor Systems (MASS)*, 2017, pp. 398–406.

[8] V. Sadhu, S. Devaraj, and D. Pompili, "Energy-efficient wireless analog sensing for persistent underwater environmental monitoring," in *Proceedings of IEEE Underwater Communications and Networking Conference (UComms)*, 2018, pp. 1–4.

[9] V. Sadhu, X. Zhao, and D. Pompili, "Energy-efficient analog sensing for large-scale, high-density persistent wireless monitoring," in *Proceedings of IEEE Wireless On-Demand Network Systems and Services*, 2017, pp. 61–68.

[10] X. Zhao, V. Sadhu, A. Yang, and D. Pompili, "Improved circuit design of analog joint source channel coding for low-power and low-complexity wireless sensors," *IEEE Sensors Journal*, vol. 18, no. 1, pp. 281–289, jan 2018.

[11] C.-C. Kao, Y.-S. Lin, G.-D. Wu, and C.-J. Huang, "A comprehensive study on the internet of underwater things: Applications, challenges, and channel models," *Sensors*, vol. 17, no. 7, p. 1477, 2017.

[12] D. M. Toma, J. del Rio, M. Carbonell-Ventura, and J. M. Masalles, "Underwater energy harvesting system based on plucked-driven piezoelectrics," in *Proceedings of IEEE OCEANS Conference*, 2015, pp. 1–5.

[13] M. E. Roberts, S. C. B. Mannsfeld, N. Queraltó, C. Reese, J. Locklin, W. Knoll, and Z. Bao, "Water-stable organic transistors and their application in chemical and biological sensors." *Proceedings of the National Academy of Sciences of the United States of America*, vol. 105, no. 34, pp. 12 134–9, aug 2008.

[14] O. Khan, A. Niknejad, and K. Pister, "Ultra low-power transceiver SoC designs for IoT, NB-IoT applications," in *Proceedings of IEEE Custom Integrated Circuits Conference (CICC)*, apr 2018, pp. 1–77.

[15] Y.-J. Kim, H. S. Bhamra, J. Joseph, and P. P. Irazoqui, "An ultra-low-power RF energy-harvesting transceiver for multiple-node sensor application," *IEEE Transactions on Circuits and Systems II: Express Briefs*, vol. 62, no. 11, pp. 1028–1032, nov 2015.

[16] E. K. Lee, H. Viswanathan, and D. Pompili, "Distributed data-centric adaptive sampling for cyber-physical systems," *ACM Transactions on Autonomous and Adaptive Systems (TAAS)*, vol. 9, no. 4, p. 21, 2015.

[17] D. Costello and S. Lin, "Error control coding," *New Jersey*, 2004.

[18] M. Rahmati and D. Pompili, "uwmimo-harq: Hybrid ARQ for reliable underwater acoustic MIMO communications," in *Proceedings of ACM WUWNET International Conference on Underwater Networks and Systems*, 2015, pp. 1–8.

[19] M. Stojanovic, "Optimization of a data link protocol for an underwater acoustic channel," in *Proceedings of IEEE OCEANS Conference*, vol. 1, no. 1, 2005, pp. 68–73.

[20] E. Soljanin, R. Liu, and P. Spasojevic, "Hybrid ARQ with random transmission assignments," *DIMACS Series in Discrete Mathematics and Theoretical Computer Science*, vol. 66, pp. 321–334, 2004.

[21] K. I. Pedersen, S. R. Khosravirad, G. Berardinelli, and F. Frederiksen, "Rethink hybrid automatic repeat request design for 5G: Five configurable enhancements," *IEEE Wireless Communications*, vol. 24, no. 6, pp. 154–160, 2017.

[22] T. Lei, M. Guan, J. Liu, H.-C. Lin, R. Pfattner, L. Shaw, A. F. McGuire, T.-C. Huang, L. Shao, K.-T. Cheng, J. B.-H. Tok, and Z. Bao, "Biocompatible and totally disintegrable semiconducting polymer for ultrathin and ultralightweight transient electronics," *Proceedings of the National Academy of Sciences*, vol. 114, no. 20, pp. 5107–5112, 2017.

[23] J. Seitner, "Analog scrambler," Feb. 2008, US Patent 7,333,608.

[24] V. Sadhu, S. Devaraj, and D. Pompili, "Towards ultra-low-power realization of analog joint source-channel coding using MOSFETs," in *Proceedings of IEEE International Symposium on Circuits and Systems*, 2019, pp. 1–4.

[25] I. F. Akyildiz, W. Su, Y. Sankarasubramaniam, and E. Cayirci, "Wireless sensor networks: A survey," *Computer Networks (Elsevier)*, vol. 38, no. 4, pp. 393–422, Mar. 2002.

[26] P. Qarabaqi and M. Stojanovic, "Statistical characterization and computationally efficient modeling of a class of underwater acoustic communication channels," *IEEE Journal of Oceanic Engineering*, vol. 38, no. 4, pp. 701–717, Oct 2013.

[27] G. Heidari-Bateni and C. D. McGillem, "A chaotic direct-sequence spread-spectrum communication system," *IEEE Transactions on communications*, vol. 42, no. 234, pp. 1524–1527, 1994.

[28] S. Azou, G. Burel, and C. Pistre, "A chaotic direct-sequence spread-spectrum system for underwater communication," in *Proceedings of MTS/IEEE OCEANS Conference*, vol. 4, 2002, pp. 2409–2415.

[29] M. Zorzi and R. R. Rao, "On the use of renewal theory in the analysis of ARQ protocols," *IEEE Transactions on Communications*, vol. 44, no. 9, pp. 1077–1081, 1996.

[30] B. Makki and T. Eriksson, "On the performance of MIMO-ARQ systems with channel state information at the receiver," *IEEE Transactions on Communications*, vol. 62, no. 5, pp. 1588–1603, 2014.

[31] M. Sherman, *Spatial statistics and spatio-temporal data: Covariance functions and directional properties*. John Wiley & Sons, 2011.